JOURNAL OF MATERIALS SCIENCE **40** (2005) 1661 – 1671

Kinetics of phase transitions and dielectric relaxations in poly-bis(trifluorethoxy-phosphazene) (PBFP)

P. VAN MOURIK*, E. VELDMAN, B. NORDER, J. VAN TURNHOUT, M. WÜBBENHORST
Delft University of Technology, Faculty of Applied Sciences, Polymer Materials and Engineering, Julianalaan 136, 2628 BL Delft, The Netherlands
E-mail: p.van.mourik2@freeler.nl

The kinetics of the high temperature (isotropic → mesophase) and low temperature (mesophase → crystalline) transition of PBFP at T_m and $T(1)$, respectively, and its local dynamics were studied by differential scanning calorimetry (DSC) at variable heating and cooling rate and by dielectric relaxation spectroscopy (DRS). While on heating no substantial effect of the rate on both transition temperatures was found, $T(1)$ and T_m showed a strong dependence on the cooling rate. The high temperature transition revealed thermally activated behaviour with an activation energy of $E_a = 400$ kJ/mol, whereas the transition at $T(1)$ showed the typical signature of supercooling. This finding is consistent with the picture that the isotropic/mesophase transition at T_m is controlled by long-range, strongly hindered, chain diffusion that leads to the long-range orientational mesomorphic order. In contrast, the low temperature transition, the enthalpy of which is far larger and the temperature of which depending linearly on the cooling rate, indicates a kinetical control by nucleation as characteristic for a (2D → 3D) crystallization process.

Complementary information about the molecular dynamics in the various phases was obtained by DRS that revealed three relaxation processes, which were assigned to the dynamic glass transition (α), local motions of CF_3—groups in the glassy state (β-process) and cooperative fluctuations of side-groups both in the mesophase and crystalline state (λ-process). Interestingly, both the Arrhenius-type β- and λ-relaxation are characterised by a non-zero activation entropy, which indicates the cooperative nature of the underlying molecular dynamics. © *2005 Springer Science + Business Media, Inc.*

1. Introduction

Polyphosphazenes are available in a wide range of properties due to a great variation of side-groups substitutions [1]. Since the synthesis of polyphosphazenes at high molecular mass was first described [2], polyphosphazenes were the subject of considerable scientific and technological interest [1]. The relation between structure and final properties is of course important for the recently developed polyphosphazenes with novel architectures [3] as well as for more "classical" polyphosphazenes, like poly-bis-(trifluoroethoxy)- phosphazene (=PBFP, see Fig. 1).

One of the striking aspects of polyphosphazenes is their combination of high-temperature stability and a wide range of values for the glass transition temperature (T_g), the latter depending on the nature of the substituted side groups [2, 4]. For polyphosphazenes, low energy barriers for rotation are mainly related with low values of T_g, e.g., PBFB combines thermal stability up to 600 K with a value for T_g of 207 K [2]. The structure of PBFP depends on the temperature. In addition to the glass transition, PBFP shows a thermotropic transformation, $T(1)$, between 330–350 K and a melting temperature, T_m, at about 500 K [5, 6]. These values appear to depend on molecular mass as well as on thermal history [5, 7, 8]. The $T(1)$-transition is attributed to side group mobilisation as well as to the onset of thermally induced backbone motions [8]. Cooling from temperatures above $T(1)$ results in highly crystalline specimens below $T(1)$ [5, 8]. Various aspects of these transitions have been reported in literature (a short overview is given in [8]). A high degree of crystallisation at temperatures below $T(1)$ is indicated by the absence of a measurable effect in the specific heat at T_g during differential scanning calorimetry DSC) [5]. However, the degree of crystallization may depend on molecular mass and thermal history [8]. Further, freshly precipitated PBFP shows a different crystalline modification

*Author to whom all correspondence should be addressed.

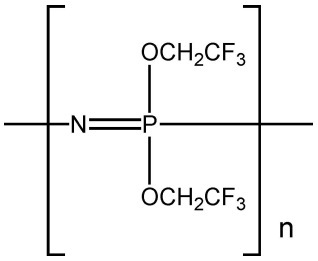

Figure 1 Schema of Poly-bis(trifluoroethoxy-phosphazene).

than after repeated heating and cooling: monoclinic vs. orthorhombic [4]. Above $T(1)$, PBFP is reported to be 2-dimensionally ordered in a pseudo-hexagonal lattice (2D) [4, 8]. At T_m, the 2D meso-phase transforms into an isotropic melt. However, strong small angle X-ray diffraction remains, indicating the persistence of short-range order above T_m [8].

Repeated heating and cooling around $T(1)$ implies repeated transformation of the pseudo-hexagonal meso-phase into the highly ordered 3-dimensional (3D) orthorhombic phase, and *vice-versa*. The kinetic parameters of transitions in PBFP (e.g., rate and temperature) are probably related to molecular rearrangements taking place in the vicinity of T_m and $T(1)$, while the transition temperatures would depend on the processing conditions [5]. Repeated passing through $T(1)$ and T_m at various cooling/heating rates may then reveal relevant factors for the kinetics of the transitions in PBFP. The results of isothermal DSC studies on the transition kinetics for PBFP indicate an extreme sensitivity to undercooling within a very short temperature range for both the transition at $T(1)$ as well as at T_m [6]. However, phenomenological knowledge on the kinetics of the transitions involved remains incomplete as these transitions were as yet usually studied at fixed heating/cooling rates or under isothermal conditions. Possible applications of PBFP inevitably imply processing, which proceeds non-isothermally rather than isothermally. Hence, from both the scientific as well as from the technological point of view, non-isothermal kinetics of the PBFP transitions is important. For the study of non-isothermal kinetics, DSC is highly appropriate [9], whereas dielectric relaxation spectroscopy (DRS) is a powerful technique for the study of molecular dynamics in most polymer materials [10, 11]. Therefore, it was decided to study non-isothermal kinetics of transitions in PBFP at different DSC cooling/heating rates in conjunction with dielectric experiments.

2. Experimental procedures

2.1. Synthesis, structure determination and differential scanning calorimetry

The synthesis was performed on the basis of reported methods [2, 12]. The yield was white fibrous polymer with a mass of 2.1 g. A film was obtained by dissolution of the fibres into acetone and subsequent casting into a PTFE mould followed by vacuum drying. The resulting film thickness was about 40 μm. For the phase identification and structure determination, a range of techniques was applied. Molecular mass was determined by Gel Permeation Chromatography (GPC) on a Waters 4510 apparatus, supplied with a styragel column, enabling the determination of the molecular mass upto 3×10^6. This GPC apparatus was calibrated with polystyrene standards. A molecular mass $M_w = 248{,}000$ was determined on a PBFP sample, the polydispersity index amounted $D = 2.45$. X-ray diffraction was performed with a High-Temperature Guinier camera and a Siemens diffractometer, applying Cu-K_α-radiation of 0.154 nm. HT-Guinier X-ray diffraction concerned heating (at 0.2 K/min) of a freshly precipitated PBFP specimen in a protecting (nitrogen) gas atmosphere. The intensity of the diffracted X-rays was photographically recorded as a function of the diffraction angle $0 < 2\theta < 30^\circ$ for temperatures between room temperature and 493 K. The diffractometer scan from a freshly precipitated specimen was obtained at ambient temperature for the same range of diffraction angles. For comparison, a scan was performed from a cyclophospazene specimen in a crystalline form. NMR measurements were performed on a Varian VXR-400S using THF as solvent.

Differential scanning calorimetry was performed on a Perkin Elmer DSC-7 apparatus. Thermal history cannot be ignored in a sequential DSC study based on one specimen. The basic advantage of such an approach is to eliminate interfering variables like variations in molecular mass or in synthesis. To eliminate variations in thermal history, cooling and heating, schemes were chosen containing at least three melting steps. The last step was followed by free cooling to room temperature (*RT*) and subsequent storage of the sample at *RT*. Calibration of the DSC apparatus was performed by measuring the melting points of mercury and indium. All results were base-line corrected. Measurements were made in an inert (nitrogen) gas atmosphere. Peak temperature deviations for the melting of indium were less than 1 K, variations in the fusion enthalpy did not exceed 0.5 J/g. The specimen was placed in an aluminium pan closed with an aluminium lid. The specimen was not removed from the pan during the DSC study. The heating/cooling rates applied were 2.5, 5, 10, 25 and 50 K/min. The temperature range studied was 173–513 K. Duplicate measurements showed that the inaccuracies in the peak integral (= enthalpy change for a certain transition) were less than 8%. The measurement scheme is shown in Fig. 2A (series A with a variation in cooling rate) and 2B (series B with a variation in heating rate). Accurate recordings were made only during the steps in which these variations were conducted: Step 7 (Series A) and 5 (Series B). However, wherever possible, values of $T(1)$ and T_m and of corresponding enthalpy changes were collected. To get information about micro-structural changes, polarisation microscopy (Jenapol equipped with Mettler hot-stage FP82) was performed on a PBFP sample prepared from the melt. Images were taken at a magnification of 200 on cooling from just above T_m. The cooling rate applied was about 10 K/min.

2.2. Dielectric measurements

Dielectric experiments were performed over 8 decades in frequency from 10^{-2} to 10^6 Hz with partially

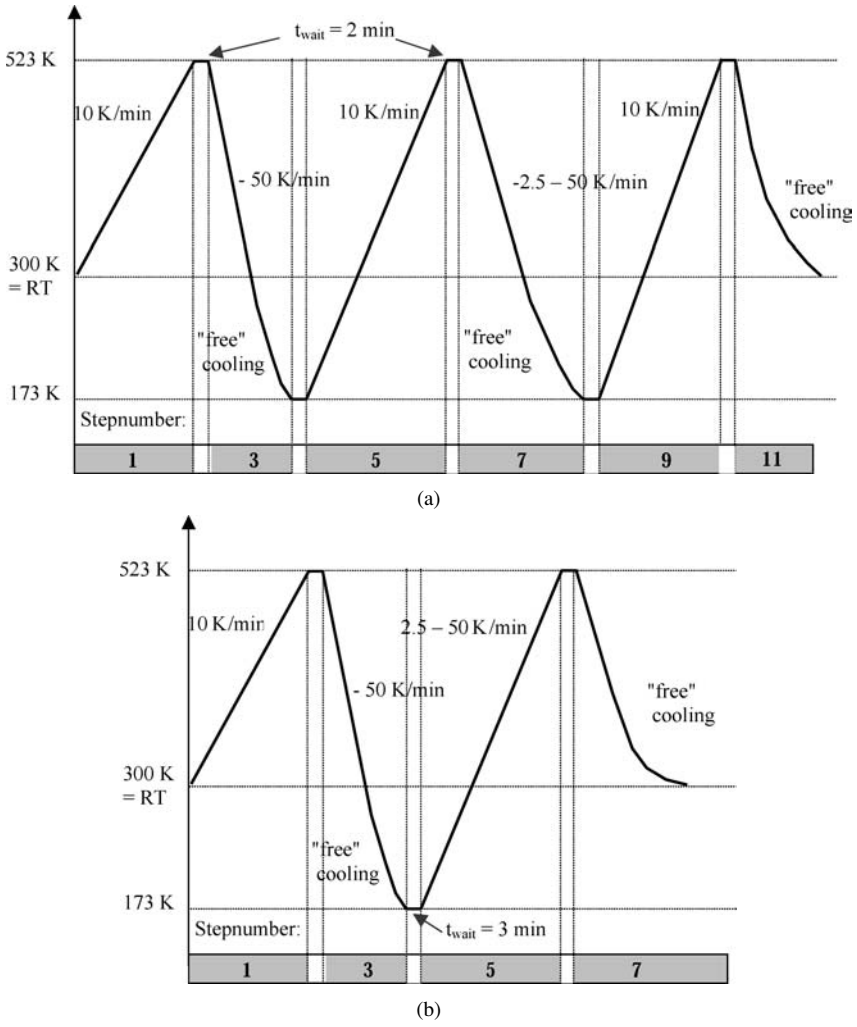

Figure 2 (a) DSC scheme for Series A: variation of cooling rate in step 7; (b) DSC scheme for Series B: variation in heating rate in step 5.

overlapping frequency ranges. For frequencies between 10^{-2} and 10^4 Hz, a frequency response analyser (Schlumberger 1260) equipped with a custom-made dielectric interface was used, while for the upper frequency range (10^2–10^6 Hz) a HP4284A precision LCR-meter was used. To obtain planar, circular samples, solid material of PBFP was heated together with quartz fibres, acting as spacers, between two circular brass plates well above T_m and subsequently cooled to room temperature under constant pressure. This procedure resulted in samples of a thickness about 50 μm and a diameter of 20 mm. For dielectric measurements, the sample was placed in a cryostat (Novocontrol), the temperature of which was controlled with an accuracy better than 0.05 K by a nitrogen gas flow. To ensure isothermal conditions during the acquisition of the dielectric spectra, the sample temperature was varied in steps typically 2.5 or 5 K, which resulted in an effective heating/cooling rate of about 0.5 K/min. More experimental details can be found in [10].

For a quantitative analysis of the dielectric data, the raw spectra were fitted to the semi-empirical Havriliak-Negami (HN) function, which enables one to account for asymmetric peak broadening by two independent shape parameters a and b [13]:

$$\varepsilon^*(\omega) = \varepsilon_\infty + \frac{\varepsilon_s - \varepsilon_\infty}{[1 + (i\omega\tau)^a]^b} \quad (1)$$

Here, ε^* is the complex permittivity, depending on the angular frequency ω, while ε_∞ and ε_s denote the high-frequency permittivity and the static permittivity. To deal with significant electrical conductivity, which is a typical feature for most polymers above their glass transition temperature T_g, we have calculated the alternative "loss" spectrum $\varepsilon''_{deriv}(\omega)$ from the real part of the complex permittivity according to Equation 2

$$\varepsilon''_{deriv} = -\frac{\pi}{2}\frac{\partial\varepsilon'(\omega)}{\partial \ln\omega}. \quad (2)$$

In contrast to the measured loss, which contains both contributions from dielectric relaxation processes and (Ohmic) conduction (characterised by "dc"-conductivity σ_{dc} according to $\varepsilon''(\omega) = \varepsilon''_{lc}(\omega) + \sigma_{dc}/\varepsilon_0\omega$), the quantity ε''_{deriv} only represents losses from relaxation terms as they are manifested in $\varepsilon'(\omega)$. A detailed description of the derivative technique and related transformations is given in [11].

For a quantitative analysis of the relaxation spectra, either ε''_{deriv} or ε'' was fitted with the corresponding expression of the HN function [derivative ε''_{deriv} (ε'_{HN}) or ε''_{HN}] yielding relaxation times and relaxation strengths for each spectrum $\varepsilon''(\omega, T)$ (see Figs 9–11).

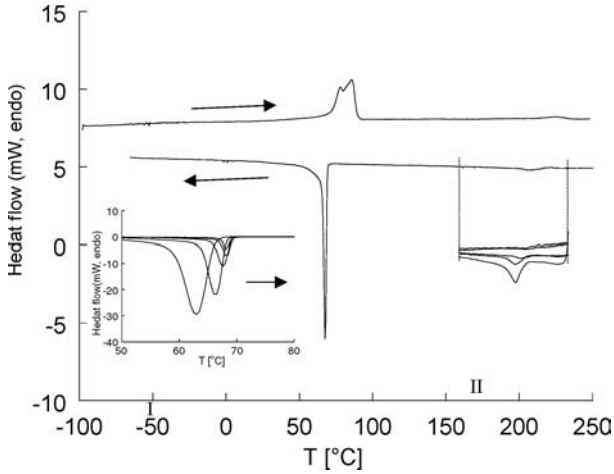

Figure 3 DSC curves as obtained in Series A Cycle 4 Step 9 (heating) and Step 7 (cooling). The two insets show the dependence on the cooling rate around $T(1)$ (inset I) and T_m (inset II).

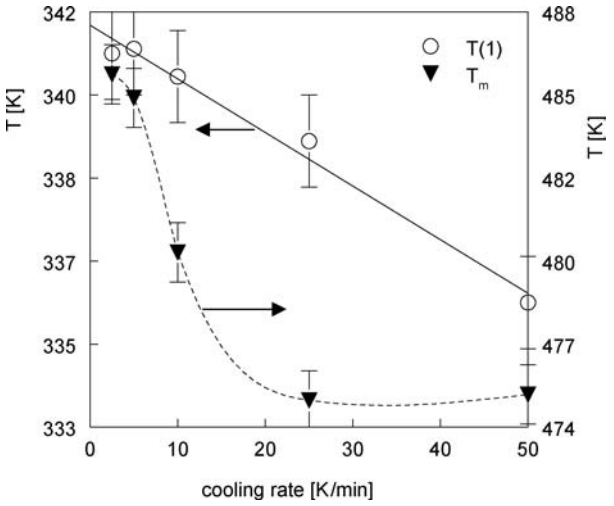

Figure 4 The values for $T(1)$ and T_m as a function of cooling rate.

3. Results

3.1. Differential scanning calorimetry, NMR and polarisation microscopy

Typical DSC curves are shown by Fig. 3, whereas Table II gathers the results of the DSC measurements. In Table III and Fig. 4, values for $T(1)$ and T_m and for the corresponding enthalpy changes, are related with the cooling rates applied. The following observations are made:

1. No dependence of values of $T(1)$ and T_m on the cycle number can be found (see Table II). Hence it is thought that these values are not influenced by cumulative thermal history.
2. On first DSC heating, the value for $T(1)$ for the freshly precipitated specimen equals about 341 K. In all other cases, this value is on heating 357 ± 4 K. On DSC heating, the T_m value equals 498 ± 2 K. These values correspond with the results obtained from HT Guinier X-ray diffraction.
3. On DSC cooling, the value for $T(1)$ is between 341 and 335 K, whereas T_m ranges from 486 to 474 K.
4. The magnitude of the enthalpy effect at $T(1)$ is much larger than at T_m.
5. At the glass transition temperature, no measurable ΔC_p-effect could be detected.
6. Careful study of the results presented in Table II—Series B reveals no relationship between heating rate and values for $T(1)$ and T_m, or with the corresponding enthalpy changes. Further, no relationship is apparently present between the values observed for $T(1)$ and T_m (and corresponding enthalpy changes) and cycle number.
7. The value of $T(1)$ and its corresponding enthalpy change decrease with increasing cooling rate. The value of T_m also decreases with increasing cooling rate. However, the enthalpy change at T_m tends to be small for low as well as high cooling rates. Note that the differences observed are at the edge of significance.
8. For Series A, the value for $T(1)$ in Step 9 is higher than in Step 5 which is higher then in Step 1. The enthalpy change at $T(1)$ on subsequent heating equals that on directly preceding cooling (compare enthalpy changes for $T(1)$ in Step 7 and Step 9 in Table II, Series A).

The NMR chemical shift values are gathered in Table I. The observed shifts do not reveal any significant indication for deviations from the known structure of PBFP. The values of $T(1)$ and T_m reported so far correspond very well with literature data (cf. [7, 14]). They were also confirmed by hot-stage polarisation microscopy. Hence, it is concluded that on cooling during polarisation between T_m and $T(1)$ the meso-phase is present and below $T(1)$ the crystalline phase is formed.

3.2. X-Ray diffraction

The X-Ray diffractometer scan of freshly precipitated PBFP is presented in Fig. 5a together with a scan

TABLE I NMR shifts for PBFP in ppm

^{1}H-nmr	Remarks	^{13}C-nmr	Remarks	^{31}P-nmr	Remarks
1.73	singlet	119.78 128.05	$\underline{C}F_3$, split quartet long-distance coupling $^3JCF_3$ = 277.2 Hz	−4.17	singlet
3.58	THF	67.98 67.60	$\underline{C}H_2$, split triplet $^2JCF_3$ = 37.9 Hz		
4.42–4.43	$C\underline{H}_2$, split quartet long distance-coupling $^3J_{HF}$ = 7.6 Hz	67.40 66.96	split triplet THF		
		64.70 63.57	split quartet THF		

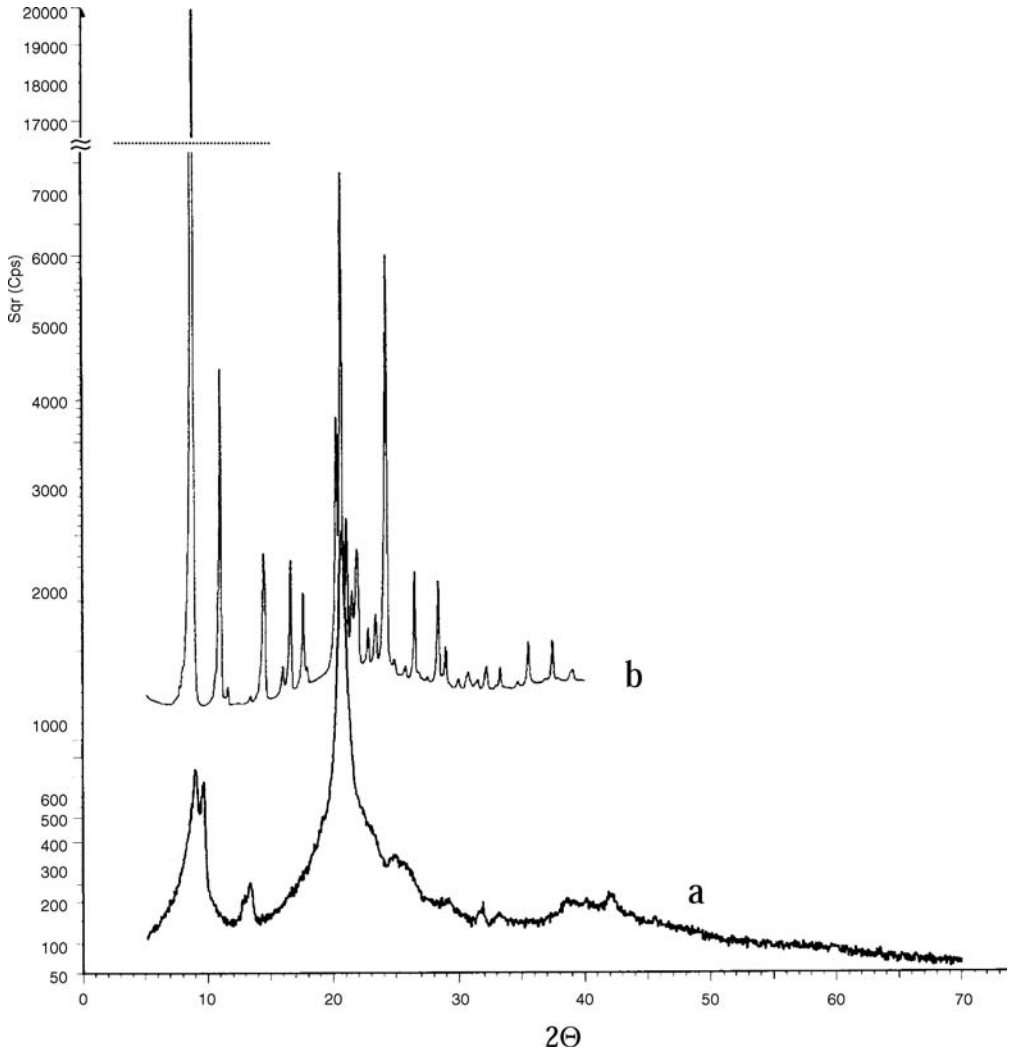

Figure 5 Diffractometer scans for semi-crystalline PBFP (a) and crystalline cyclophosphazene (b).

for crystalline cyclophosphazene (b). On heating, HT-Guinier X-ray diffraction yielded $T(1) = 339 \pm 5$ K and $T_m = 493 \pm 10$ K. By digitizing the HT-Guinier photograph, various diffraction scans at individual temperatures were extracted which are displayed in Fig. 6.

The following observations are made:

For Fig. 5

The diffractometer peaks for the cyclophosphazene show an increased peak/background ratio compared to the corresponding peaks for the PBFP specimen. Hence, the PBFP specimen cannot be considered as fully crystalline. However, the overall appearance (with sharp peaks strongly present) of the diffractometer scan indicates a high degree of crystallinity.

For Fig. 6

At about 333 K the ratio between the maximum intensities at $2\theta \approx 10^\circ$ and at $2\theta \approx 20^\circ$ changes from less than unity to larger than unity. On increasing the temperature, the peak at about $2\theta \approx 10^\circ$ broadens significantly around 483 K, an effect that already happens at about 333 K for the peak at $2\theta \approx 20^\circ$. Above this temperature, the peak corresponding to a spacing of about 1.0 nm

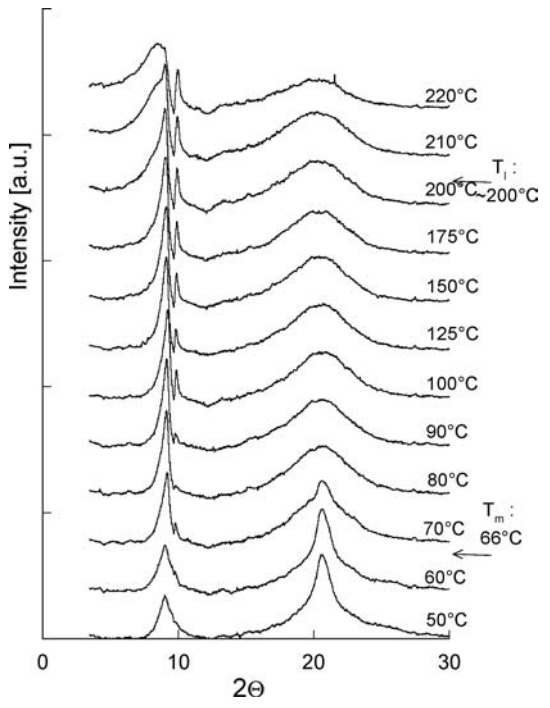

Figure 6 X-ray diffraction intensity as a function of diffraction angle 2θ for various temperatures obtained from a HT Guinier experiment.

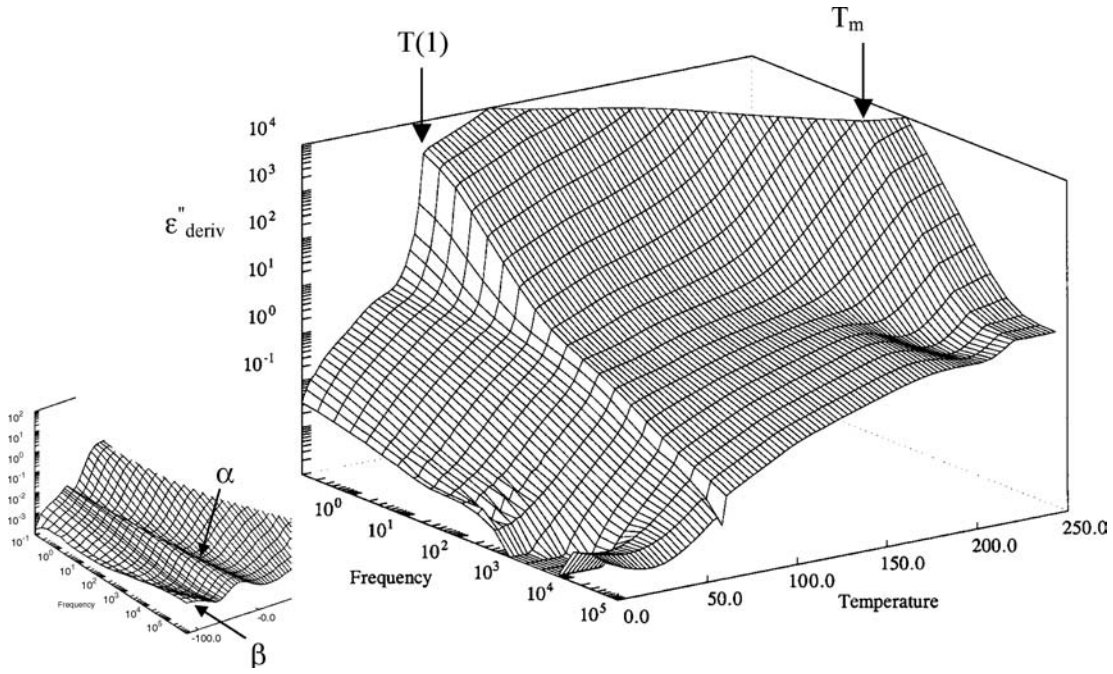

Figure 7 3D-representation of the conduction-free loss $\varepsilon''_{\text{deriv}}$ of PBFP during cooling from 523 K.

remains present, although the melt is generally described as isotropic [4].

3.3. Dielectric measurements

A 3D representation of the conduction-free loss $\varepsilon''_{\text{deriv}}$ for PBFP on cooling is given in Fig. 7, the inset shows the loss ε'' in the glass transition region. Both spectra reveal various relaxation phenomena and the two thermal transitions at $T(1)$ and of T_{m}, which manifest themselves as sharp, frequency independent changes in the dielectric response. The values for $T(1)$ and of T_{m} (360 and 500 K on heating, 340 and 480 K on cooling) agree well with those obtained from DSC (cf. Table II) and show a slight hysteresis between heating and cooling.

Three dielectric relaxation processes were found, which were denoted β, α and λ in the order from low to high temperatures. The Arrhenius presentation (Fig. 8) of the relaxation time dependence $\tau(T)$ allows the classification of molecular relaxations into "simple" thermally activated processes (τ obeys the Arrhenius law $\ln\tau = \ln\tau_\infty + E_{\text{a}}/RT$) and relaxations obeying the Vogel-Fulcher-Tammann (VFT) relation $\ln\tau = \ln\tau_\infty + E_{\text{a}}/R(T - T_{\text{V}})$ which is characteristic for the dynamic glass transition. Here, T_{V} is the (Vogel) reference-temperature, and R is the gas constant.

The β-relaxation, visible at the low temperature/high frequency edge in Fig. 8, shows Arrhenius behaviour with a low activation energy $E_{\text{a}} = 31$ kJ/mol typical for localised molecular motions. In contrast, the α-process clearly reveals the typical VFT-curvature in the τ vs. $1/T$ plot which is indicative for cooperative relaxations associated with the dynamic glass transition in PBFP.

At temperature somewhat below $T(1)$ and in the whole temperature range of the mesophase ($T(1) < T < T_{\text{m}}$), another relaxation process λ was revealed by the fit techniques described before. This process changes strongly on passing $T(1)$, while in the mesophase regions an Arrhenius-like behaviour is identified (cf. Fig. 9). Obviously, this process is sensitive to the degree of molecular order that changes during the

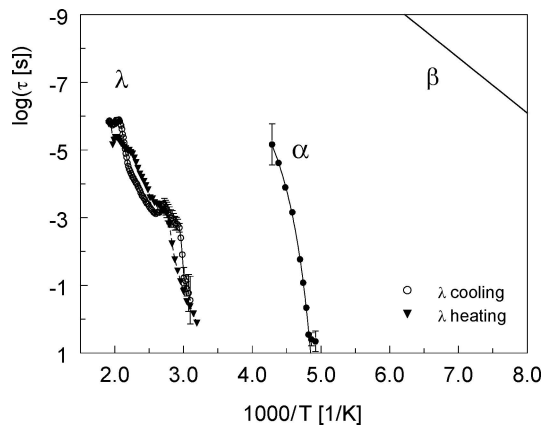

Figure 8 Activation plot for all dielectric relaxation processes found in PBFP.

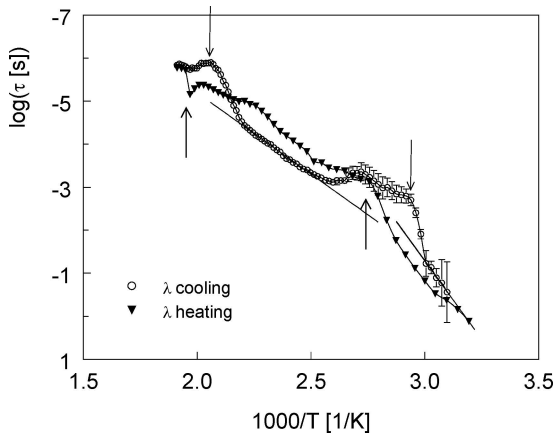

Figure 9 The relaxation time $\tau(T)$ as a function of the reciprocal temperature for the $T(1)$ and T_{m} transitions.

TABLE II DSC results

	Series A												*Series B*				
	Step 1		Step 5		Step 7					Step 9				Step 5			
	$T(1)$ (K)	ΔH (J/g)	$T(1)$ (K)	ΔH (J/g)	Cooling rate	$T(1)$ (K)	ΔH(J/g)	T_m (K)	ΔH (J/g)	T(1)(K)	ΔH(J/g)	T_m(K)	ΔH(J/g)	Heating rate	$T(1)$ (K)	ΔH (J/g)	T_m (K)	ΔH (J/g)
Cycle 1	340.7	12.3	354.4	+30.2	*25*	339.2	−27.9	474.9	−1.7	356.1	+26.5			*50*	355.9	31.6	499.9	+2.3
Cycle 2	353.6	26.2	358.5	+31.6	*10*	340.6	−28.4	479.9	−1.5	358.6	+28.3			*25*	354.5	31.2	499.3	+2.7
Cycle 3	354.1	27.3	356.3	+32.7	*5*	341.1	−29.7	485.1	−1.6	357.6	+28.6	497.6	+1.5	*10*	353.8	32.7	498.3	+1.4
Cycle 4	354.2	27.2	354.6	+32.5	*2.5*	341.1	−30.3	485.9	−3.0	356.3	+31.4	496.6	+1.8	*5*	353.5	32.4	496.0	+1.7
Cycle 5	351.7	27.5	354.3	+32.0	*50*	335.7	−28.0	475.1	−2.1	354.1	+27.0			*2.5*	354.2	30.6	498.7	+4.8

TABLE III Cooling rate and values for $T(1)$ and T_m

	T(1)		T_m	
Cooling rate K/min	Position	Enthalpy change (J/g)	Position (K)	Enthalpy change (J/g)
2.5	341.1	−30.3	485.9	−3.0
5	341.2	−29.7	485.1	−1.6
10	340.6	−28.4	479.9	−1.5
25	339.2	−27.9	474.9	−1.7
50	335.7	−28.0	475.1	−2.1

transition from 3D to 2D order. However, it should be noted that the temperature dependence of the relaxation time of the λ-process may reflect two phenomena: (i) true thermal activation of molecular motions for a given molecular structure, and (ii) changes in the molecular packing reflecting the kinetics of the phase transitions. Therefore activation parameters were deduced from the $\tau_\lambda(T)$ dependence (see Fig. 9) exclusively at temperatures sufficiently far from $T(1)$ and T_m.

4. Discussion

4.1. Dielectric relaxation processes

In a previous section we have identified three dielectric relaxation processes being present in PBFP, denoted α, β and λ. We will now discuss the α-relaxation in more detail.

From the VFT-behaviour, indicated by a curved graph $\log(\tau)$ vs. $1/T$ (cf. Fig. 8), we have concluded that the α-process is the dielectric manifestation of the dynamic glass transition involving the PBFP backbones. Extrapolating the VFT-fit curve to a relaxation time $\tau(T_g) = 100$ s allows to determine an operationally defined glass transition temperature, which usually is in fair agreement with T_g values as determined by DSC. In this way, a T_g value of 205 K was obtained for PBFP, which is very close to that ($T_g = 207$ K) reported by [2]. It should be noted that there are only a few T_g data available from the literature, most likely because of the high crystallinity of PBFP at temperatures below $T(1)$ which gives rise to only small ΔC_p-effects in the calorimetric response. This property of many polyphosphazenes, reaching rather high degrees of crystallinity (up to 90% [5]) is also manifested in the dielectric results shown in Fig. 10. Here, the upper curve reveals a sharp drop in the high frequency permittivity at $T(1)$, indicating that most of the mobile polymer fraction is frozen-in upon crystallization. A simple analysis of the $\varepsilon'(T)$ steps around T_g and $T(1)$ yields a crystallinity of at least 80%. Despite this high crystallinity, the dielectric α-process, although weak in intensity, does obviously not suffer from the presence of a chain extended crystalline phase. In other words, the remaining amorphous polymer fraction still exhibits bulk dynamics implying the existence of amorphous regions well separated from the crystalline phase.

In contrast to the α-process, the β-relaxation clearly obeys the Arrhenius law, which, in combination with the low activation energy of $E_A = 31$ kJ/mol, supports its assignment to local motions within the PBFP structure. However, the pre-exponential factor $\log(\tau_\infty) = -19$ is far from a value typical for "true" local motions ($\log(\tau_\infty) \sim -12$ [16]) exclusively involving simple energy barriers (e.g. bond rotational potentials).

An interesting approach to interpret the activation parameters of the dielectric relaxations has been suggested by Starkweather [16]. Based on the Eyring equation for absolute reaction rates, he proposed an analysis which enables the evaluation of the *activation entropy* ΔS and the zero-entropy activation energy $E^*_{A,0}$ from the experimental Arrhenius parameters E_A and τ_∞. He derived an expression (Equation 3),

$$E^*_A = RT'\left(1 + \ln\frac{k_B}{2\pi h} + \ln\frac{T'}{f}\right) + T'\Delta S_A \qquad (3)$$

which predicts the apparent activation energy E^*_A as a function of the activation entropy ΔS_A and the temperature T', which is the temperature of the relaxation peak maximum at the frequency $f = 1$ Hz. In case of $\Delta S_A = 0$, Equation 3 yields the so-called zero-entropy activation energy $E_{A,0}$. From the same expression, inserting the experimentally determined activation energy, we obtain the activation entropy at the temperature T' according to Equation 4:

$$\Delta S_A = \frac{1}{T'}\left[E_A - RT'\left(1 + \ln\frac{k_B}{2\pi h} + \ln\frac{T'}{f}\right)\right] \qquad (4)$$

According to Starkweather, non-cooperative (local) motions are characterised by a negligible activation entropy, whereas cooperative relaxations possess a non-zero ΔS value. This classification can be rationalized by the assumption that the degree of molecular order determines the degree of cooperativity of a particular motional process, which is related with local order perturbations implying entropy fluctuations. A positive activation entropy then signifies that the motional process requires a temporary higher disorder in its excited state. Equations 3 and 4 have been applied to the Arrhenius-type relaxation processes in PBFP, the results are summarised in Table IV.

From Table IV it becomes clear that the β-relaxation shows a substantial degree of cooperativity while its zero-entropy activation energy is very low (∼20 kJ/mol). Although the detailed molecular mechanism associated with the dielectric β-process is not

TABLE IV Activation parameters for dielectric relaxation processes in PBFP

Process	T_V (K)	E_V (kJ·mol^{-1})	$\log(\tau_\infty)$	E_A (kJ·mol^{-1})	$E_{A,0}$ (kJ·mol^{-1})	ΔS (kJ·mol^{-1}K^{-1})
β	–	–	−19.1	31.2	20.3	0.12
α	188.0	3.60	−9.3	–	–	–
λ (mesophase)	–	–	−12.7	72.4	75.4	−0.01
λ (cryst.)	–	–	−23.2	140.0	77.8	0.19

TABLE V Relevant data for the Kissinger analysis

Cooling rate	T_m	$1000/T_m$	$\ln(T_m)^2/\lvert\phi\rvert$
2.5	485.9	2.0580	11.4557
5	485.1	2.0614	10.7593
10	479.9	2.0838	10.0446
25	474.9	2.1057	9.1073
50	475.1	2.1048	8.4150

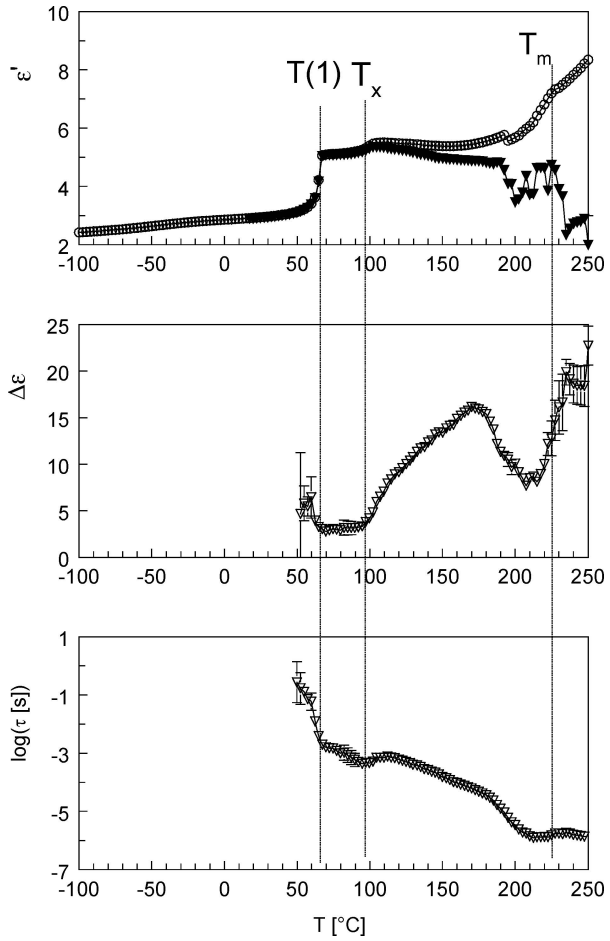

Figure 10 High frequency permittivity ε_∞ (top, triangles), relaxation strength of the λ-process $\Delta\varepsilon_\lambda$ (middle) and relaxation time τ_λ (bottom) obtained from fits of the dielectric spectra $\varepsilon'(f)$ and $\varepsilon''_{\text{deriv}}(f)$. For comparison, the measured permittivity at 480 kHz is shown as well (top, circles).

known yet (cf. results and discussion given in [17]), the high activation entropy implies that the relaxation process involves somehow cooperative reorientations of the CF_3-groups.

Let us now focus on the λ-relaxation which was assigned to highly correlated motions involving the CF_3-groups in the *crystalline* and the *mesophase*. This process, which shows up directly in Fig. 7, reveals a strong discontinuity at $T(1)$ in the relaxation time $\tau(T)$ (cf. Figs 8 and 9) while the relaxation strength $\Delta\varepsilon(T)$ drops to some extent at the crystalline → mesophase transition (cf. Fig. 10). Well separated from the discontinuity around $T(1)$, the relaxation time was fitted to an Arrhenius law both *below* and *above* $T(1)$ and subsequently analysed using Equations 3 and 4. As expected, the measured activation energy E_A drops when the system undergoes a transition from the crystalline state to the mesophase. Interestingly, this change is almost exclusively caused by a change in activation entropy, while the zero-entropy activation energy $E_{A,0}$ remains practically unchanged (75.4 vs. 77.8 kJ/mol). In other words, upon changing from a 3D to a 2D positional order, the λ-process obviously looses its high cooperativity indicating that the gain in translational mobility results in the vanishing of severe sterical hindrance.

Inspection of Fig. 10 reveals another interesting feature in the dielectric properties of PBFP: At about 100°C, a discontinuity in both $\Delta\varepsilon(T)$ and $\tau_\lambda(T)$ shows up, which suggests the existence of a possible, phase transition between different mesophases. At the present stage one can only speculate about the existence of such a transition, since more experimental evidence is needed to confirm a fine-structure in the mesophase of PBFP.

4.2. Transitions at $T(1)$ and T_m on heating and cooling

The PBFP X-ray diffractometer scan (Fig. 5) corresponds fairly well with the data given by Nakamura [8] for a PBFP specimen of rather low molecular mass ($M_w = 5 \times 10^4$). Nakamura *et al.* [8] suggested that the presence of the monoclinic phase be at least partly related with the average molecular mass of the specimen concerned. The corresponding value for the present specimen was 2.5×10^5 with a polydispersity index of 2.45. According to [8] the value for $T(1)$ for the first heating was 346 K, to compare with the present 341 K (see Table II). Flory-Fox plots give the relation between the value of $T(1)$ and/or T_m and molecular mass [7]. The present value for $T(1)$ corresponds well to the literature data quoted. It is commonly observed that on first heating the value of $T(1)$ is lower than on repeated heating and that the difference between first and second heating is of the order of 10 K [5]. The present results are in perfect correspondence. Apparently, chain unfolding and the onset of backbone mobility start easier from the monoclinic than from the orthorhombic state, although differences in molecular mass as well as degree of crystallisation may exert a certain influence [7, 8].

The crystallinity above $T(1)$ contributes to the crystallinity below $T(1)$ [5]. Sequential melting and cooling increases $T(1)$, see point 8. in Section 3.1 and see Table II. However, the value of $T(1)$ does not depend on the cycle number. Clearly, chain alignments are maintained during the rather short times of melting, but are lost on prolonged storage at room temperature at the end of a cycle.

On heating, the values for $T(1)$ and T_m as obtained from dielectric measurements in virtually isothermal conditions (see Section 3.3) and from HT-Guinier X-ray diffraction (see Section 3.2) with a very low heating rate of 0.2 K/min, agree with the ones obtained by DSC. It is already noted that transitions in PBFP are related with rearrangements of side groups and/or backbone segments. Compared to the heating rates applied, rearrangement rates on a molecular scale will always be fast. No relation between values for $T(1)$ and T_m and DSC heating rates applied could be established. This excludes kinetics solely governed by thermal activation

[9]. Apparently, at the present experimental conditions, neither the $T(1)$ nor the T_m transition show a rate dependent kinetics.

Above the melting point, the interactions between the backbones are weaker, yielding a broadening of X-ray diffraction peaks (see Fig. 6). However, strong small angle X-ray diffraction remains. Hence, it can be said that on passing T_m only small adjustments in the molecular packing occur, implying only small enthalpy changes, as is observed. In the solid state, the full width at half maximum (FWHM is inversely related to the X-ray correlation length) of the inner X-Ray diffraction peak with a spacing of about 1.0 nm is not very sensitive for a variation in molecular mass [8]. Above T_m, FWHM for a higher value of M_w is smaller than for a lower value of M_w, while T_m itself is lower for a lower value of M_w. Hence, it is assumed that ordering in the solid state is primarily determined by the mutual packing of the backbones.

On cooling, the transition from the melt to the 2D meso-phase is determined by the cooling rate (see Fig. 4). However, crystallization usually presumes long-scale chain diffusion allowing a thermal nucleation & growth process. Apparently, the curvature of the plot in Fig. 4 reflects the occurrence of thermal activation, in contrast with the transition at $T(1)$ on cooling. Assuming a temperature of a fixed stage of an thermally activated transition and that the relevant thermodynamic and kinetic parameters are constant within the temperature range studied, the relation between cooling rate, peak temperature and reciprocal temperature takes the form of the so-called Kissinger-equation [18]. At the transition temperature, T_m, the relaxation time τ for the λ-relaxation eaches a minimum (cf. Fig. 9, where log τ is plotted against the reciprocal temperature). The occurrence of such an extreme can be related with the rate of temperature change [19]. Supposing that this minimum corresponds to a fixed transition stage, the Kissinger analysis is applied in the present case (see Table V). Then, an activation energy of about 400 kJ/mol is obtained to be compared with 125 kJ/mol for LLDPE, 160 kJ/mol for PHBA (as derived from the data given by Chuah *et al.* [20]) and 328 kJ/mol for nylon 11 [18]. Apparently, the steric hindrance in combination with dipole-dipole interactions and H-bonding due to the side groups contribute effectively to the value of the activation energy.

The linear relation between $T(1)$ and the cooling rate (see Fig. 4) disproves the role of thermal activation at this transition, i.e., this transition kinetics is solely governed by the supercooling attained. The larger the cooling rate was, the lower the temperature of transition and hence the smaller the amount of transformed phase as is shown by the negative relation between the value of ΔH and the cooling rate (cf. Table III). The foregoing implies that the enthalpy change induced by the $T(1)$-transition evolves suddenly instead of gradually, which is indeed found (compare the curves on heating and on cooling in Fig. 3). During the transition, the 2D chain extended mesophase transforms into a 3D orthorhombic chain extended form [8]. The observed kinetic differences for the λ-relaxation are related with highly correlated motions involving CF_3-groups in the crystalline and meso-phase (see Section 4.1). Hence, the transition involved is thought to proceed via the displacements of the CF3-containing side groups to perform this 2D/3D rearrangement.

5. Conclusions

1. The kinetics of the high temperature (isotropic → mesophase) transition of PBFP is controlled by a long-range, strongly hindered, chain diffusion (at an activation energy of about 400 kJ/mol) that leads to the long-range orientational mesomorphic order.

2. The kinetics of the low temperature (mesophase → crystalline) transition of PBFP shows the typical signature of supercooling indicating that this transition is controlled by nucleation as characteristic for a (2D → 3D) crystallization process.

3. DRS revealed three relaxation processes, which were assigned to the dynamic glass transition (α), local motions of CF_3–groups in the glassy state (β-process) and cooperative fluctuations of side-groups both in the mesophase and crystalline state (λ-process).

4. Both the Arrhenius-type β- and λ-relaxation are characterised by a non-zero activation entropy, which indicates the cooperative nature of the underlying molecular dynamics.

5. For the (3D) crystalline phase, a large value for the activation entropy and for the apparent activation energy; whereas for the (2D) meso-phase, a rather small value for the apparent activation energy with a non-zero entropy activation energy.

6. Extrapolation of the relaxation time data for the α-relaxation, obeying the VFT-law, yielded a value for T_g corresponding very well to literature data.

Acknowledgements

Mr. P. Droppert is acknowledged for his assistance in the dielectric experiments. X-ray measurements were performed by ing. N.M. van der Pers and Mr. J.H. van Lent (Laboratory of Material Sciences and Technology, Delft University of Technology). NMR measurements were conducted by Dr. A. Sinnema and Dr. J.A. Peeters (Department of Chemical Technology, Delft University of Technology).

References

1. H. R. ALLCOCK, *Phosph., Sulfur Silicon* **144–146** (1999) 61.
2. H. R. ALLCOCK, R. L. KUGEL and K. J. VALAN, *Inorg. Chem.* **5** (1966) 1709.
3. H. R. ALLCOCK, N. J. SUNDERLAND, RAVIKIRAN and J. M. NELSON, *Macromolecules* **31** (1998) 8026.
4. S. G. YOUNG, M. KOJIMA, J. H. MAGILL and F. T. LIN, *Polymer* **33** (1992) 3215.
5. D. C. SUN and J. H. MAGILL, *ibid.* **28** (1987) 1243.
6. R. J. CIORA and J. H. MAGILL, *Macromolecules* **23** (1990) 2350.
7. M. L. WHITE, R. A. MONTAUE, K. MATYJASZEWSKI and T. PAKULA, *Polymer* **36** (1995) 3493.
8. H. NAKAMURA, T. MASUKO, M. KOJIMA and J. H. MAGILL, *Macromol. Chem. Phys.* **200** (1999) 2519.
9. M. J. STARINK, Delft: Delft University of Technology, 1992.

10. I. J. A. MERTENS, M. WÜBBENHORST, W. D. OOSTERBAAN, L. W. JENNESKENS and J. VAN TURNHOUT, *Macromolecules* **32** (1999) 3314.
11. M. WÜBBENHORST and J. VAN TURNHOUT, *J. Non-Cryst. Solids* **305** (2002) 40.
12. H. R. ALLCOCK, J. E. GARDNEER and K. M. SMELTZ, *Macromolecules* **8** (1975) 36.
13. S. HAVRILIAK, JR. and S. J. HAVRILIAK, "Dielectr. Mech. Relax. Mater." (Hanser, Munich, 1997).
14. I. C. CHOY and J. H. MAGILL, *J. Polym. Sci.* **19** (1981) 2495.
15. I. N. SHTENNIKOVA, G. F. KOLBINA, S. V. BUSHIN and A. Y. VOLKOV, *Russ. J. Appl. Chem.* **73** (2000) 1269.
16. H. W. STARKWEATHER, *Polymer* **32** (1991) 2443.
17. I. MURAKAMI, H. OCHIAI, K. TOMINAGA and M. KAJIWARA, *J. Inorg. Organomet. Polymers* **2** (1992) 255.
18. M. L. DI LORENZO and M. L. SILVESTRE, *Prog. Polym. Sci.* **24** (1999) 917.
19. A. BOERSMA, J. VAN TURNHOUT and M. WÜBBENHORST, *Macromolecules* **31** (1998) 7453.
20. K. P. CHUAH, *Polymer* **40** (1998) 253.

Received 5 January
and accepted 19 October 2004